WATER RESOURCES RESEARCH, VOL. 34, NO. 4, PAGES 869–877, APRIL 1998

Calculation of average landslide frequency using climatic records

Leslie M. Reid

USDA Forest Service Pacific Southwest Research Station, Redwood Sciences Laboratory, Arcata, California

Abstract. Aerial photographs are used to develop a relationship between the number of debris slides generated during a hydrologic event and the size of the event, and the long-term average debris-slide frequency is calculated from climate records using the relation. For a site in California with an average of 8.3 slides km^{-2} yr^{-1}, a sequence of four photo sets (representing 10–15 years, 35–50 observed slides, and 4–6 large storms) is needed to estimate the long-term debris-slide frequency to within 30% of the actual value ($p = 0.90$). If climatic records are used, a record length of 5–10 years (17–35 observed slides and 2–4 significant storms) is sufficient to provide the same accuracy. The climate-based model suggests that debris-slide frequency changed from approximately 1.6 to 8.3 slides km^{-2} yr^{-1} during the late 1930s owing to an increased frequency of high-intensity storms. The model accurately predicts the change in slide-scar density observed on sequential aerial photographs following the climatic shift.

1. Introduction

Estimates of average long-term rates of landsliding are often needed for sediment budget calculations or for comparisons of erosional characteristics in different areas or under different land-use conditions. Estimates are usually calculated from long periods of record, as when the number of new landslides is counted on sequential aerial photographs and the total is divided by the years separating the first and last photo sets [e.g., *Reid et al*., 1981]. This method can provide valid estimates of a long-term average frequency if the sampling period includes an average distribution of landslide-producing events. However, the photographic period usually either overrepresents or underrepresents the frequency of large events. Because climatic records commonly are available for longer periods than aerial photographic coverage, it would be useful to be able to calculate long-term landslide frequencies from climatic data. This paper describes such a method and uses data from a field site in central California as an example. Although the area sampled is small, it is useful for illustrating the method and for demonstrating the types of temporal patterns in landslide frequencies that can be identified using the method.

2. Study Site

Landslides were mapped in a 41-ha area in the hills between Pinole and Martinez, California (Figure 1) during a study of gully initiation [*Reid*, 1989]. The Simas Valley field site is underlain by Tertiary marine sandstone and shale and supports a vegetation cover of scattered oaks and non-native annual grasses. Hillslope soils are silt-clay mollisols and vertisols that develop cracks as wide as 5 cm during the dry season. Hillslopes have an average slope of 22°, but valley bottoms are broad terraces of Quaternary alluvium (Figure 1). Hillslopes have been grazed by cattle since the area was ceded as a land grant in the 1840s, and parts of the alluvial terraces were cultivated for dryland grain and hay until the 1940s.

Rainfall in the area is strongly seasonal, with 77% of the precipitation falling between the beginning of October and the end of April. The average annual rainfall at the field site is approximately 550 mm [*Contra Costa County Public Works Department*, 1977], but annual totals vary widely from year to year. Annual rainfall at San Pablo Reservoir, 5 km away, has ranged between 250 and 1400 mm over the 77-year period of record to 1994. Work by *Nilsen et al*. [1976] suggests that debris slides in similar parts of the San Francisco Bay area are triggered by rainfall in excess of 180 mm during a single storm. Examination of the rainfall record from San Pablo Reservoir shows an uneven distribution of calendar months having more than 180 mm of rain (Figure 2), suggesting that landslides would need to be inventoried over many decades to produce a valid estimate of landslide frequency.

Most of the landslides in Simas Valley are shallow debris slides, but approximately 17% are shallow earthflows, and another 20% are more deeply seated slumps and channel undercuts. Only the debris slides are considered in the following analysis. The debris slides are distinctive in that they remove only the upper 50–60 cm of soil above a planar failure surface. The mobilized sediment usually liquefies and flows from the slope, leaving an evacuated slide scar, a pair of marginal levees downslope of the scar, and a veneer of sediment on the otherwise undisturbed surface between the levees. Superelevated deposits left on the opposite valley wall after a moderate-sized flow suggest that flows may reach velocities of nearly 4.5 m s^{-1} at the base of the slope [*Reid*, 1989]. In February 1986, debris slides were observed during high-intensity rain bursts following several weeks of storms.

3. Mapping and Dating Landslides

New debris-slide scars were mapped on each of seven aerial photograph sets on 41 ha of hillslopes. In addition, fresh slide scars were mapped on the first photograph set (1939), and the scars of debris slides that occurred between the date of the last photo set (1980) and the summer of 1983 were mapped in the field over a portion of the 41-ha area. Slide scars were again field mapped during the summer of 1986 (Table 1). In each case, bottomlands underlain by Quaternary alluvium were excluded from the mapping and are not considered in calcula-

Paper number 97WR02682.

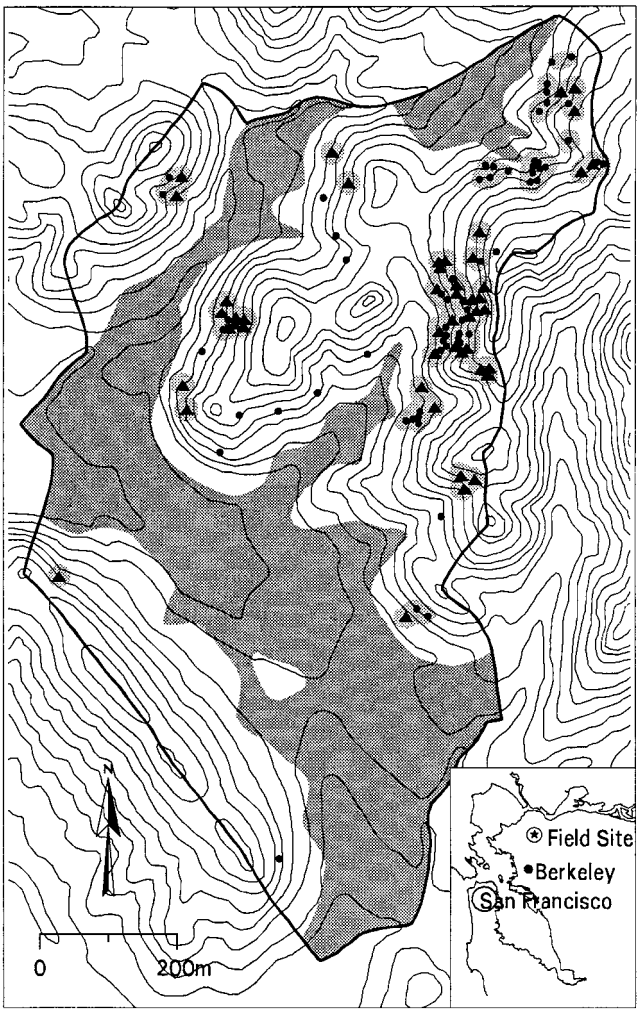

Figure 1. Location of debris-slide scars visible between 1939 and 1986 in a portion of Simas Valley, California. Dark shading indicates alluvial deposits; light shading indicates the area within 13 m of at least two slide scars; triangles indicate reactivated scars; and dots indicate nonreactivated scars.

tions of landslide densities and frequencies; values are thus reported per unit area of hillslope.

Scales of the photographs range between 1:9200 and 1:24,100, so survey results reflect some variance due to differences in resolution. However, comparison of debris-slide scars mapped from the 1:20,000 photographs taken in 1950 with those mapped from the 1:10,000 photographs of 1953 shows little difference even for the older scars, and few large storms occurred between the two photograph dates. This agreement suggests that scale differences are not a major source of variance. Additional variance is introduced because scars are most easily seen on photographs taken in the spring while grass is short and green. Slide scars are thus expected to be most easily recognized on the 1:12,800 photo set from March 1974 (Table 1).

Field observations show that slide scars are quickly revegetated by grasses and herbs which take root on interrill areas even as rilling continues on the scar surface. Each slide scar was categorized according to the extent of revegetation, and the duration of each recovery category was estimated by comparing categorization of the same slide scars on sequential photo sets (Table 2). Where a slide scar in an intermediate age class was not seen on a photograph but was visible on the preceding and following photo sets, it was assumed to have been overlooked on the intervening photograph, and the record was treated as continuous for determining the duration of visibility. The number of overlooked scars is listed in Table 1 for each photo set, and the 30 overlooked scars represent about 4% of the total number of observations. More than 75% of the overlooked scars fell into the two oldest age classes.

Comparisons show that scars are usually revegetated after about 7 years, and more than 90% of the closely age-bracketed scars were revegetated by 9 years after their occurrence. The 16 unvegetated scars mapped on the 1939 photo set were thus assumed to have been caused by storms that had occurred since 1930. Summing the duration of the age categories suggests that on average, a debris-slide scar will remain visible on aerial photographs for a minimum of about 40 years. The average period over which scars are recognizable is actually longer, since many of the older scars remained visible at the end of the period of record and so could be used only to estimate minimum durations. The minimum durations that were longer than the averages calculated using only scars that vanished during the period of record are included in the recalculated averages in Table 2.

Mapping of debris-slide scars also demonstrated that slides often recur at the same site. Seventy-six of the 160 debris slides that occurred between 1939 and 1983 were located on or immediately adjacent to older scars. On this basis, scars that remained unvegetated for more than 9 years after the major hydrologic event in the photo interval were assumed to represent multiple slide events; this assumption applies to eight of the catalogued debris slides. In some cases reactivation appears to have simply deepened an existing scar without changing the area excavated. On average, debris slides recur a minimum of 18 years after the previous failure at a given site, and several sites show four periods of reactivation. The proportion of slides that occurred on or adjacent to visible slide scars increased from 35% in 1946 to about 60% in 1986, and this pattern will be further examined in the following discussion.

Summing the number of debris slides that occurred between sequential photographic sets and those between 1980 and 1986 produces an estimated long-term average debris-slide frequency on hillslopes of 8.4 slides km^{-2} yr^{-1}. However, the 1953–1959 photo interval alone accounted for nearly one quarter of the observed slides, so it was prudent to determine

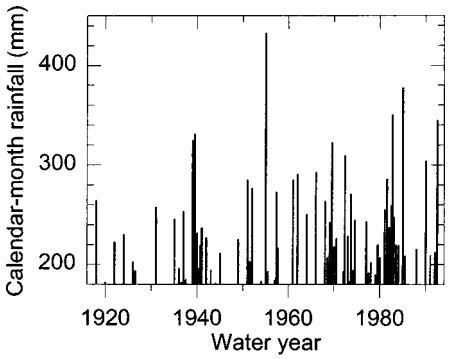

Figure 2. The distribution of 1-month rainfalls greater than 180 mm at San Pablo Reservoir, California, between 1917 and 1994.

Table 1. Data Sets Used to Calculate Frequencies of Debris Slides

Date	Record Type	Scale	Area Surveyed, ha	New Slides	Density of New Slides, slides km^{-2}	Interval, years	Total Slide Density, slides km^{-2}	Overlooked Scars
Aug. 2, 1939	air photo	1:20,900	41.0	16*	39.0	9*	110	1
Sept. 6, 1946	air photo	1:24,100	41.0	26	63.4	7	154	0
March 3, 1950	air photo	1:20,200	41.0	10	24.4	4	149	4
Aug. 15, 1953	air photo	1:10,000	41.0	7	17.1	3	149	5
June 30, 1959	air photo	1:9,200	41.0	43	104.9	6	205	4
July 2, 1968	air photo	1:13,000	41.0	5	12.2	9	195	7
March 4, 1974	air photo	1:12,800	41.0	20	48.8	6	217	0
July 15, 1980	air photo	1:12,600	41.0	3	7.3	6	185	6
June 1983	field	···	33.3	30	90.1	3	228	3
June 1986	field	···	30.6	19	62.1	3	216	0
Total				179	469.3	56		30

*Debris slides that showed little revegetation of the slide scar were counted; these are assumed to have occurred during the previous 9 years (see text).

whether underrepresentation or overrepresentation of large storms had distorted the long-term average. This was done by relating areal debris-slide density to an index of storm size and using this relationship to calculate the number of slides expected from each storm event of the climatic record, as described in the following sections.

4. Relating Areal Debris-Slide Density to Storm Size

Rainfall data between 1917 and 1983 were available as monthly totals for the gauge nearest Simas Valley. Some storms thus will be partitioned into 2 months, and their overall impact underestimated. Records from 1983 to 1994 show that individual storms that dropped more than 100 mm of rain lasted an average of 7 days, but that over 30% of the storm's rain fell on a single day even for the largest storms, and about 50% fell over 2 consecutive days. Because the days with the highest intensity were generally near the middle of the storm period, there will be only about a 1-in-30 chance that less than about 75% of a storm's rainfall will not be tabulated in a single month. On the other hand, the overall impact of small storms will be overestimated when multiple storms occur within a calendar month.

Several indices (maximum 1-month, 2-month, and annual rainfall for the photo interval) were tested against areal debris-slide densities for each photo interval to find the highest correlation using linear, quadratic, and cubic least squares regression models. In cases where the index maximum for the interval was within 10% of the value of other events during that interval, the slide density was divided by the number of "maximum events" during the interval (Table 3). For example, if two events of 325 and 331 mm (e.g., 1-month rainfalls for the 1946 photo set, Table 3) occurred during an interval in which the next largest event was less than 298 mm, half of the slides were attributed to each of the two largest events. In this case the halved debris-slide total would then be plotted against the average size of the two maximum events (the "averaged maximum 1-month rainfall"). The 1974 sample set provides an additional data point because the absence of fresh debris-flow tracks indicates that no debris slides had occurred before March during the 1973–1974 water year.

Implicit in this approach are the assumptions that the largest events are disproportionately responsible for triggering debris slides and that the occurrence of debris slides does not affect later sliding rates. The first of these assumptions is tested and supported by the method described here. The second is unlikely to be true, but the nature of the influence is unclear. Later rates may be lessened because unstable sites are "used up" by evacuation of mobile material, or they may be increased because the occurrence of a slide destabilizes adjacent slopes. In either case the assumption is not critical to the success of the method because the assumption is used only to provide a first estimate of the relation.

Comparison of the resulting least squares regression plots of areal slide density versus the various rainfall parameters identified the maximum 1-month precipitation within the photo-

Table 2. Age Categories for Debris-Slide Scars and Mean Durations

Category	Characteristics	*n*	Percent Representing Minima*	Mean Duration, Years	Range in Duration, Years	Standard Deviation, Years
A	debris track visible	···	···	···	···	···
B	scar unvegetated	···	···	···	···	···
A + B	(combined duration)†	77	6	6.2	3–13.5	1.9
C	scar vegetated, but distinct	91	12	7.8	3–25.5	3.7
D	subdued topography	69	20	11.8	3–38	8.4
E	little evidence	37	32	11.1	3–30	8.2
Total				36.9		

*Percent of samples for which only a minimum duration could be determined. Because of the high percentages noted for categories D and E, the durations listed probably underestimate the actual mean.

†Photo intervals were too long to determine duration of categories A and B independently.

Table 3. Maximum 1-Month Rainfalls for Debris-Slide Sample Intervals

Air-Photo Date	Rainfall Date	Maximum Rainfall, mm month^{-1}	Averaged Maximum Rainfall, mm month^{-1}	Total Debris Slides	Adjusted Debris Slides*	Adjusted Debris-Slide Density,* slides km^{-2}
Aug. 2, 1939	Dec. 1931	258	252	16	5.3	13.00
	Feb. 1936	246	···	···	···	···
	Feb. 1938	253	···	···	···	···
Sept. 6, 1946	Jan. 1940	325	328	26	13.0	31.71
	Feb. 1940	331	···	···	···	···
March 3, 1950	Jan. 1950	226	226	10	10.0	24.39
Aug. 15, 1953	Jan. 1952	285	281	7	3.5	8.54
	Dec. 1952	277	···	···	···	···
June 30, 1959	Dec. 1955	433	433	43	43.0	104.88
July 2, 1968	Feb. 1962	285	290	5	1.7	4.07
	Oct. 1962	291	···	···	···	···
	Jan. 1967	293	···	···	···	···
March 4, 1974	Jan. 1970	323	316	20	10.0	24.39
	Jan. 1973	310	···	···	···	···
1973–1974 water year†	Nov. 1973	229	229	0	0.0	0.00
July 15, 1980	March 1974	271	258	3	1.5	3.66
	March 1975	245	···	···	···	···
June 1983	March 1983	350	350	30	30.0	90.09
June 1986	Feb. 1986	378	378	19	19.0	62.09

*The number of debris slides divided by the number of maximum rainfall events.
†This interval could be characterized because no fresh scars were present on the 1974 photographs.

graphic interval as the most useful index of those tested. It is possible that a finer rainfall reporting interval might produce a stronger correlation, but the potentially important effects of antecedent moisture may not be accounted for if too short an index interval is selected.

The plots also provided preliminary estimates of the relationship between areal debris-slide density and the rainfall index, but these relations hide the effects of multiple high-rainfall months occurring in each photographic interval. The following iteration method was thus used to extract the underlying relationships between the slide density for a month and the rainfall occurring during that month.

The preliminary linear, quadratic, and cubic least squares regression fits between total slide density and maximum 1-month rainfall for photo-bounded sampling intervals were adopted as the first estimates of the underlying relationships between 1-month slide density and 1-month rainfall. The preliminary relationships were used to calculate the number of debris slides associated with each month's rainfall over the period of record. The total density of debris slides predicted for the entire measurement period (56 years) was then divided by the total density observed (469 slides km^{-2} for the 56 years), and the predictive relations were normalized by this ratio to account for the fact that the original relations assigned all slides to the few largest storms. In essence, the total number of observed slides is distributed among the storms that occurred between 1930 and 1986.

Monthly debris slides were then recalculated using the revised equations, and the monthly estimates were summed for each photo-bounded sampling interval. Comparison of predicted and observed slides for each of the 11 intervals then provides a test of the adequacy of the linear, quadratic, and cubic prediction models. Each of these relations was then iteratively modified using a brute-force algorithm (Figure 3) to optimize the predictive power of the equation, until the relation between predicted and observed slides in the photo intervals attained a slope of 1.0 and an intercept of 0.0 (Figure 4). The cubic fit was found to provide the most accurate predictions:

$$L = (0.0143P - 1.82)^3 \qquad P > 127$$
$$L = 0 \qquad P \le 127 \tag{1}$$

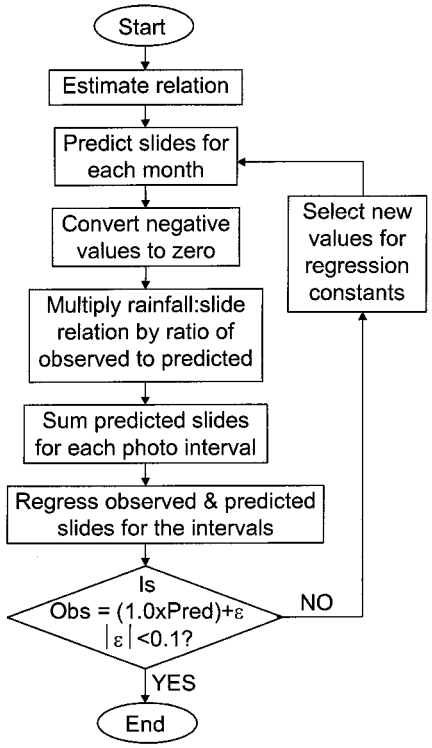

Figure 3. Algorithm for defining a relation between debris-slide densities and rainfall amounts.

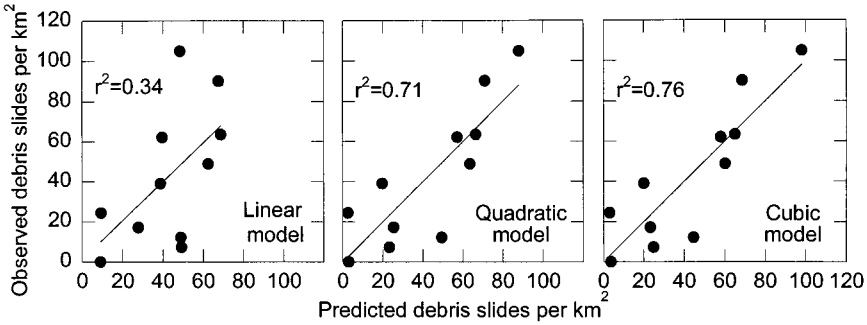

Figure 4. Comparison of predicted and observed debris slides in sampling intervals; the r^2 is shown for each test. Predictions are based on underlying linear, quadratic, and cubic models.

where L is the areal debris-slide density (slides km^{-2}) for a given month and P is the corresponding 1-month rainfall (mm). The resulting relationship between predicted and observed debris slides for the photo intervals has a slope of 1.000, an intercept of 0.000, and a coefficient of determination (r^2) of 0.76. Equation (1) was thus selected as the estimator for debris-slide density. The average error for the individual predictions is 14 slides km^{-2} per interval, with the average error for predicted values of more than 50 slides km^{-2} in an interval being about half that for lower values.

All 11 photograph- and field-based observation intervals were used to develop (1). To provide an independent test of the approach, the relation was recalculated 11 times with a different combination of 10 observation intervals. Each equation was then used to predict the number of slides expected for the interval not used in constructing the equation. The resulting regression between predicted and observed slides provides a coefficient of determination of 0.61 and an average error of 17 slides km^{-2}, with the magnitude of the error again markedly smaller for intervals with many slides.

5. Calculation of Average Debris-Slide Frequency

Climatic records were then evaluated to determine the distribution of 1-month rainfalls over the 77-year period of record (1917–1994). Rainfall event magnitudes were tabulated to estimate the long-term average rainfall frequency as a function of event size. Values greater than 100 mm in a month were plotted as a cumulative curve and smoothed by eye (Figure 5). The resulting curve was used to calculate the expected number of months falling in each rainfall interval in a year. In compiling the relation it became evident that the character of storms changed in the mid to late 1930s, and examination of a plot of cumulative months of rainfall greater than 200 mm revealed a zone of inflection between 1934 and 1939. Frequencies thus were also compiled separately for 1917–1938 and for 1939–1994 (Figure 5), with the break point selected to correspond to the first year of aerial photography. Comparison of the curves shows an increased frequency of high-rainfall months after 1938.

Debris-slide frequencies for the average year were then calculated for each rainfall interval using (1). For example, the debris-slide density generated by a maximum 1-month rainfall between 290 and 300 mm (14.0 slides km^{-2}, calculated using (1) for 295 mm) was multiplied by the frequency of such an event (0.0024 of all months, from the relation for 1917–1994 in Figure 5, multiplied by 12 months yr^{-1}) to yield 0.40 slides km^{-2} yr^{-1} for that type of event. Such a calculation was repeated for the other rainfall intervals and the results were summed to obtain the long-term average frequency of 6.4 slides km^{-2} yr^{-1} (Figure 6). In this case the long-term average calculated from the 77-year climatic record is about 25% lower than the value of 8.4 slides km^{-2} yr^{-1} calculated using the 56-year span of aerial photographs and field observations.

Because the average frequency calculated directly from the aerial photo observations reflects the post-1938 period of higher 1-month rainfall intensities, the average debris-slide frequency was recalculated using the rainfall distribution characteristic of 1939–1994. The calculated frequency for this period is 8.3 slides km^{-2} yr^{-1}, which agrees well with the photo-based estimate. This agreement is not unexpected, since (1) was designed to optimize interval predictions for the actual

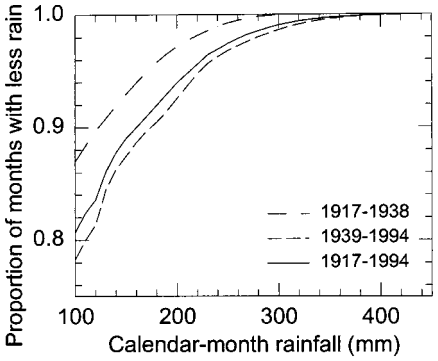

Figure 5. The distribution of 1-month rainfalls for 1917–1938, 1939–1994, and 1917–1994.

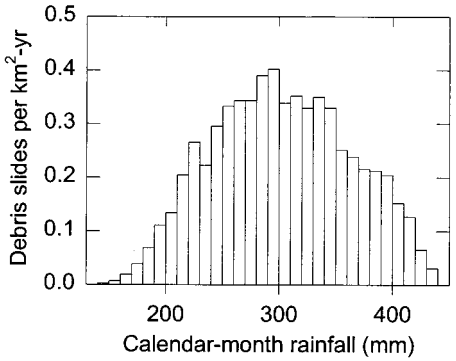

Figure 6. Average distribution of debris slides by rainfall interval for 1917–1994.

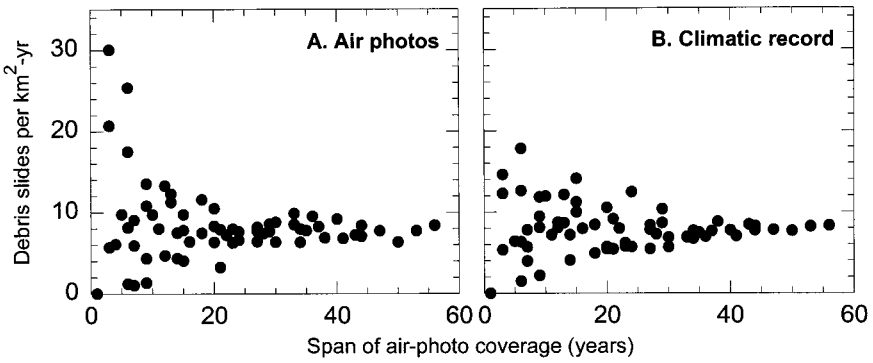

Figure 7. The effect of record length on estimated debris-slide frequency for the Simas Valley area for (a) the air-photo-based method and (b) the climatic record–based method.

rainfall record, and the cumulative rainfall distribution used in the calculation is derived from the actual rainfall record for essentially the same period.

The cubic model suggests that rainfall of over 200 mm in a calendar month is necessary to generate at least one debris slide per square kilometer. Even though rainfalls of over 350 mm in a month can generate more than 30 slides per square kilometer, such storms are infrequent enough that they contribute only about 25% of the debris slides in the long run. In contrast, 1-month rainfalls of 280–300 mm are the most effective landslide producers. This interval alone appears to be responsible for 12% of the debris slides in the area.

6. The Effect of Record Length on Estimated Average Debris-Slide Frequencies

The Simas Valley area is atypical in having a 40-year sequence of aerial photographs taken at relatively short intervals. This record makes it possible to determine how the accuracy of long-term landslide frequency estimates is affected by the length of the observation record. Average debris-slide frequencies were thus calculated for every possible interval length (e.g., 1946–1950, 1946–1953) represented by the air-photo sets and field observations by dividing the density of new slides by the duration of the interval (Figure 7a). In this case a record of at least 30 years is required to average out the effects of short-term weather fluctuations even though landslides are frequent, storms capable of generating landslides occur approximately seven times a decade, and half the debris slides are caused by storms that occur more than four times a decade. In areas with less frequent slide-producing events, correspondingly longer periods of record would be required to obtain a valid estimate of long-term average slide frequencies.

The ability to calculate long-term rates using the climatic record–based method also is reduced where the air-photo record is abbreviated, since data from multiple photo sets are used to define the relation between slide frequency and climate indices. Relations between areal slide density and 1-month rainfall were thus constructed independently for the sequence of observations included in every possible photo- and field-based observation interval, and average slide frequencies were calculated for each of the resulting relationships by applying them to the 1939–1994 climatic record (Figure 7b). For spans characterized by only one or two photo intervals, an additional data point was provided by the field observation that a month contributing 150 mm of rain produced no debris slides. Spans represented by two or three data points were represented by linear models, while those with more information were characterized using cubic models. One span that produced an anomalous relationship (a negative slope) due to the lack of large storms was excluded from the analysis.

Comparison of standard deviations of average slide frequencies for various air-photo spans suggests that the climate-based method provides a better estimate of average frequencies than does the photo-based method if data are few (Figure 8). In this case the two methods produce similar results after 10–15 years of air-photo record are available, which is equivalent to about three photographic intervals. Comparability is achieved over a time span long enough to include four to six modal slide-generating events (250–350 mm in a month) and 35–50 new slides. The improved predictive power of the climate-based method is due largely to its ability to make use of the short air-photo record to enable interpretation of the much longer rainfall record in terms of debris-slide generation and thus to make use of a more accurate characterization of the distribu-

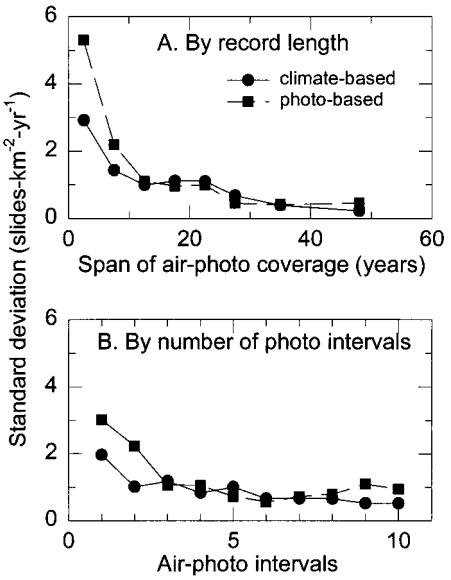

Figure 8. Standard deviations for estimated long-term debris-slide frequencies calculated using air-photo-based and climatic record–based methods as a function of (a) record length and (b) number of photo intervals.

tion of slide-generating storms than is possible using the period of air-photo records alone.

If this sample size is representative of data requirements for other areas, the required measurement durations for those areas can be estimated. For example, in 1977 the 15-km^2 upper Christmas basin on the Olympic Peninsula in Washington had a frequency of road-related shallow debris slides of approximately 0.06 per road kilometer per year with a road density of 2.4 km km^{-2} [*Reid*, 1981]. Generation of 35 to 50 new slides in the watershed would thus require 16–25 years at that road density. This duration is of the same order as the air-photo span to present (1971–1995) and the length of time that road densities have been greater than 2.0 km km^{-2} (1974–1995). Thus it is likely that until the mid-1990s, estimates of debris-slide frequency would have been better made by constructing a relationship between a climatic index and air-photo-based measurements of landslide densities in the Christmas Creek area than by using air-photo-based frequency estimates alone.

7. Comparison of Model Formulations

Estimated average debris-slide frequencies were compared for the linear, quadratic, and cubic relations between slide density and 1-month rainfall to test the sensitivity of the estimates to the complexity of the selected form of the model. Average rates were calculated for air-photo records progressively truncated from 1986 to represent the types of records likely to be available for California Coast Range conditions (Figure 9). The similarity of estimates using linear, quadratic, and cubic models was unexpected. The optimized quadratic and cubic models turned out to be nearly identical for the parts of the rainfall spectrum that produce most of the slides. Divergence of these models at higher values of rainfall has little influence on the estimated total frequency because such high rainfalls rarely occur. Agreement by the linear model was more fortuitous. In this case, overestimates for slide densities at low rainfall values were compensated by underestimates at higher values. The relative weakness of the linear model is evident from its lesser ability to predict debris-slide densities for specific intervals (Figure 4).

The stability of the model estimates for long-term averages is due largely to the fact that most debris slides occur during moderate rainfall events. The quadratic and cubic models suggest that more than 50% of the slides occur during months with rainfalls of 250–350 mm. As the data set is progressively truncated, the fitted models vary most in their treatment of the extreme parts of the distribution, which do not strongly influence the overall average.

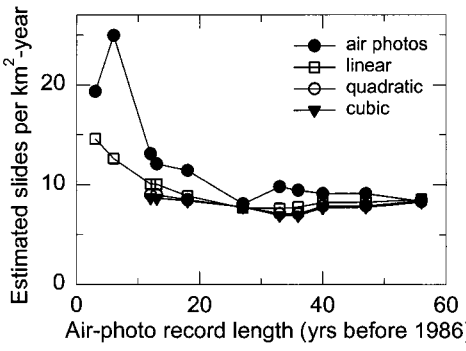

Figure 9. Effect of progressively truncated aerial-photographic records on estimates of the long-term average debris-slide frequency.

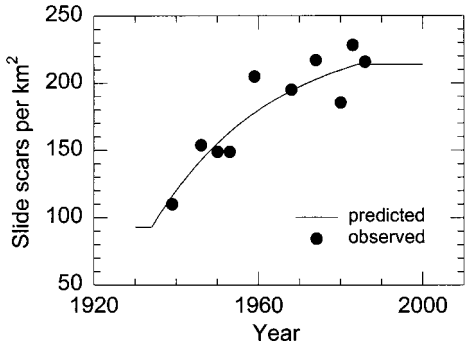

Figure 10. Observed and predicted densities of debris-slide scars.

8. Variations in Debris-Slide Frequency Through Time

Even where a lengthy aerial photographic record is available, it cannot be used in isolation to determine the effects of longer-term shifts in weather patterns that can strongly influence estimates of long-term debris-slide frequencies. In the present case the early part of the 20th century was drier and had fewer slide-generating storms than the period for which an air-photo record is available. Average rates calculated from debris-slide densities observed on aerial photographs thus cannot be applied to the period predating about 1939 (Figure 2). Examination of long-term climatic records from San Francisco (1849 to present) and Sacramento (1878 to present) suggest that the conditions represented by the 1917–1938 period began in about 1890 and were interrupted only by a period of higher intensity storms around 1915. The average annual frequency of debris flows between 1917 and 1938 can be estimated by applying (1) to climatic records from that period. Results show an estimated frequency of 1.6 slides km^{-2} yr^{-1}, a decrease to 25% of the average for the full 77-year period.

This change in debris-slide frequencies is reflected in a progressive change in the total number of slide scars visible on sequential aerial photographs (Figure 10). If the average landslide frequency and the average period over which scars are visible were both constant over time (i.e., if there were no changes in variables such as climate or land use that would cause a fundamental change in the temporal distribution of landslide densities or healing rates), then the rate at which new scars appear must equal the rate at which old ones disappear. In this case the number of scars present would produce a stable average through time; the actual number present would vary from year to year, but the long-term average would show no longer-term trend. This average scar density ($\bar{N}$, scars km^{-2}) would equal the average number of new scars created each year, multiplied by the effective lifespan of the scar (A_T, years):

$$\bar{N} = R_T(1 - P_r)A_T \tag{2}$$

where R_T (slides km^{-2} yr^{-1}) is the debris-slide frequency for both new and reactivated scars and P_r is the probability that a given slide will have occurred on a still-visible scar. The effective lifespan takes into account the proportion of scars that are

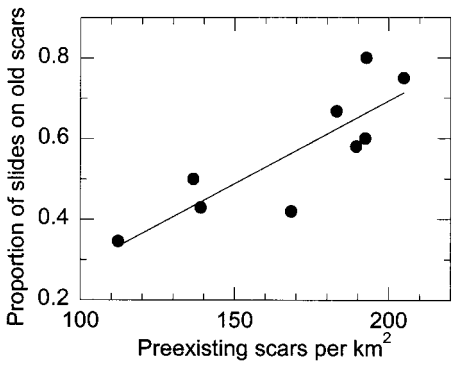

Figure 11. Proportion of new debris slides occurring on old scars as a function of scar density.

reactivated before healing. If reactivation is assumed to occur randomly over the lifespan of a scar (or if the average age at reactivation is half the average lifespan of the scar, as is suggested by the distribution of reactivation ages) and the probabilities of subsequent reactivations are independent of one another, then the effective lifespan can be calculated from the average lifespan of scars that are not reactivated (A_n, years):

$$A_T = A_n \sum_{i=0}^{\infty} \left(1 + \frac{i}{2}\right)(P_r^i - P_r^{i+1}) = \frac{A_n}{2}\left(\frac{2 - P_r}{1 - P_r}\right) \quad (3)$$

where the terms summed over the index i (which corresponds to the number of sequential reactivations at a site) account for the influence of repeated reactivations of the same scar. In essence, the average lifespan for nonreactivated scars is multiplied by their proportion of the total slides ($A_n(1 - P_r)$) and added to the average lifespan for once-reactivated scars multiplied by their proportion ($1.5A_n(P_r - P_r^2)$), and so on.

The proportion of scars reactivated has been changing through time and is most closely correlated with the density of slide scars that existed before the slides occurred (N_o; Figure 11):

$$P_r = 0.00409N_o - 0.125 \qquad r^2 = 0.71 \quad (4)$$

Figure 2 suggests that climatic conditions had already begun to change by 1939, so a characteristic scar density for the earlier period was estimated by subtracting from the observed 1939 scar density (110 scars km^{-2}) the $39 \times (1 - 0.325)$ new scars that formed between 1930 and 1939 (where 39 scars km^{-2} is the observed density of new scars from Table 1 and 0.325 is the earliest observed proportion of reactivated scars), and adding back the $1.6 \times (1 - 0.325) \times 9$ scars that would, on average, have disappeared during the same 9-year period (where 1.6 slides km^{-2} yr^{-1} is the estimated debris-slide frequency before 1939). The calculation produces an estimated scar density of 93 scars km^{-2} that would have been present in 1930. Applying (4) to the calculated scar density produces an estimated probability of reactivation of 0.255, and this value allows (2) to be used to calculate an effective scar lifespan of 78 years. Equation (3) then produces an estimated lifespan for nonreactivated scars of 67 years, about 1.8 times the minimum estimated in Table 2. However, this value provides an overestimate of the lifespan because scars from the cluster of storms around 1915 would still have been visible in 1939.

A third estimate of scar lifespan is possible from examination of the changes in the frequency of disappearing scars through time. If the storms of the mid-1930s initiated a period of accelerated landslide formation, then a corresponding period of scar disappearance should have begun between about 37 and 66 years later. This period appears to have started in about 1980, suggesting a lifespan on the order of 45 years. This value, too, may underestimate the actual lifespan because the sample period is as yet too short to ensure that the rate has stabilized. In any case an average lifespan of 50 years is assumed in the following calculations.

The trend of scar density through time (Figure 10) suggests that a density of about 93 scars km^{-2} would have last been seen in the mid-1930s, corresponding to the time of the first cluster of large storms since the rainfall record began (Figure 2). If the new slide regime is assumed to have started in 1935, then the calculated landslide rates and reactivation probabilities (from (4)) can be used to estimate the number of scars visible as a function of time (Figure 10). Predicted values agree well with those observed on aerial photographs and in the field. The ultimate landslide scar density is expected to be approximately 210 scars km^{-2} of hillslope, assuming a constant climate.

The strong dependence of the probability of reactivation on the scar density (Figure 11) suggests that only a limited proportion of the total area is prone to landsliding. Were this the case, the number of scars present divided by the proportion of new slides occurring on old scars would be constant for each observation period, and would equal the number of available sites. The average for nine observations is 380 sites km^{-2}, with a standard error of 13 sites km^{-2}. The debris-slide scars have an average area of 60 m^2, and slides that overlapped the old scars were classified as reactivations. Thus the area represented by each "site" is equal to an area with twice the radius of the average slide scar, or approximately 240 m^2. A population of 380 "sites" per square kilometer implies that 9% of the hillslope area is highly slide-prone.

Slide-prone areas were independently mapped as areas in proximity to at least two slide scars: All but 15 of the 206 debris-slide scars in the area were located in the 8.7% of the hillslope area within an average of 1.5 mean slide diameters (13 m) of at least two debris slides (Figure 1). Comparison of a plot of the cumulative number of reactivated scars and the values predicted assuming that there are only 380 potentially unstable sites shows close agreement between predicted and observed values and thus supports the utility of the assumption (Figure 12). Cumulative values were used rather than specific values to obviate the need to recalculate scar populations prior to each landslide-generating event.

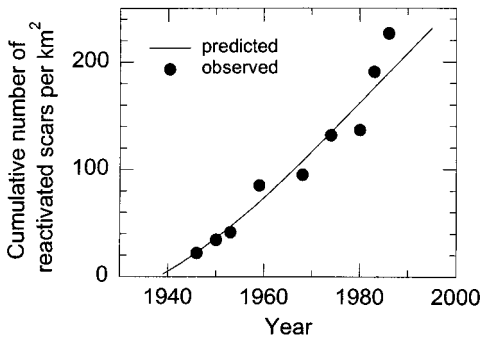

Figure 12. Observed and predicted cumulative proportion of debris slides on reactivated scars.

9. Conclusions

When landslide data are limited, the use of climatic records to calculate landslide frequencies from aerial photo surveys provides a more stable estimate of long-term average frequencies than does estimation using aerial photographs alone. Where climatic conditions have not changed, the climate-based estimates were found to require only about half the record length to provide estimates of the same order of accuracy as those obtained using the aerial photographs alone. Both methods make use of areal landslide densities measured from air photos or fieldwork, but the climate-based method "leverages" this information by relating the observed landslide densities to climatic indices. This relationship can then be used to calculate long-term average landslide frequencies from rainfall records, which are usually considerably longer than the available air-photo records. Thus the climate-based method provides estimates that are relatively insensitive to short-term weather fluctuations, while estimates calculated from the photo record alone represent only the weather conditions spanned by the air-photo record.

Even if the aerial photo record is long enough that the climate-based method provides no predictive advantage, the method is useful because it furnishes additional information about conditions that control landslide generation. Where climate patterns have changed, for example, the climate-based method allows estimation of the effect of the change on slide frequencies. This type of calculation is generally not possible using aerial photographs alone because the maximum record length is usually too short.

For the area considered here the accuracy of the climate-based method does not depend strongly on the form of the model used to describe the relation between slide densities and a rainfall index. As long as the model provides a reasonable estimate of the central range of the relation, where most landslides are generated, the overall averages are relatively consistent. Models vary more in their ability to predict the effects of major events, but these have a relatively minor influence on the long-term averages because of the rarity of such events. However, this pattern should serve as a warning that the models cannot be applied with confidence to predict the effects of isolated high-intensity storms. In this case, for example, the model predicts that the very wet January 1995 would have generated a large number of landslides. Field observations after the storm, however, showed an unexpectedly low debris-slide density both at the Simas Valley site, where observed slide densities were an order of magnitude lower than predicted, and through much of the central California Coast Ranges (T. Spittler, personal communication, 1995). In the case of the Simas Valley site, exclusion of grazing from the area 3 years previously may have affected the landslide density, but the regional extent of the unexpected response indicates that other factors, as yet unknown, more strongly influenced the response. Thus correlative models may be useful for describing average conditions, but even a well-defined model must be used with extreme caution if the response to a specific event is to be predicted.

Results for the case considered show that there has been an increase in landslide frequency since 1939 and suggest that this difference is associated with a change in weather patterns. Drier conditions and lower maximum rainfall intensities before 1939 were associated with an average debris-slide frequency that was approximately 25% of the rate characteristic of the period following 1939. During the present period, more than 50% of the debris slides in the area are generated during months having 250 to 350 mm of rain, and these occur, on average, about 3 times a decade. It is possible that a change in climatic conditions also could have been associated with other changes. Wetter conditions could have led to increased cattle stocking densities because of better forage conditions, for example, or they could have produced a shift in the species composition of the grasslands. Thus, although the association between weather patterns and landslide frequency suggests a causal relation, it is not an adequate demonstration of cause.

Calculation of average frequencies from climatic records is particularly effective in the present case because slide-generating storms occur frequently, debris-slide frequencies are high, a lengthy rainfall record exists, and many air-photo sets are available for the study area. The method will give less accurate results in areas with less frequent landslides or fewer air photos, but so will any method for estimating long-term frequencies. In any area where climatic records are lengthier than records of landslide occurrence, however, it is likely that using climatic information in calculations of long-term slide frequencies, whether those calculations be based on field observations or on aerial-photographic surveys, will strengthen the estimates and provide information useful for interpreting those estimates.

Acknowledgments. Robert Nuzum of the East Bay Municipal Utility District arranged access to the field area. Al Puffer of the National Weather Service (Eureka) and staff of the EBMUD Hydrology Division provided rainfall records. Fieldwork was partially supported by grants from the National Science Foundation and the USDA Forest Service Pacific Northwest Research Station. R. Jacobson, A. Howard, and B. Morgan provided helpful comments.

References

Contra Costa County Public Works Department, Mean seasonal isohyets compiled from precipitation records 1879–1973, *Contra Costa County Flood Control Water Conserv. Dist. Drawing Number B-166*, Martinez, Calif., 1977.

Nilsen, T. H., F. A. Taylor, and E. E. Brabb, Recent landslides in Alameda County, California (1940–71): An estimate of economic losses and correlations with slope, rainfall, and ancient landslide deposits, *U.S. Geol. Surv. Bull*., *1398*, 21 pp., 1976.

Reid, L. M., Sediment production from gravel-surfaced forest roads, Clearwater Basin, Washington, *Publ. FRI-UW-8108*, 247 pp., Univ. of Wash. Fisheries Res. Inst., 1981.

Reid, L. M., Channel incision by surface runoff in grassland catchments, Ph.D. dissertation, Univ. of Wash., Seattle, 1989.

Reid, L. M., T. Dunne, and C. J. Cederholm, Application of sediment budget studies to the evaluation of logging road impact, *J. Hydrol. N. Z*., *20*, 49–62, 1981.

L. M. Reid, USDA Forest Service Pacific Southwest Research Station, Redwood Sciences Laboratory, 1700 Bayview Dr., Arcata, CA 95521. (lmr7001@axe.humboldt.edu)

(Received February 9, 1996; revised September 11, 1997; accepted September 19, 1997.)